Title

Structure of a Mycobacterium tuberculosis Heme-Degrading Protein, MhuD, Variant in Complex with Its Product

Journal

Biochemistry, 58(46)

ISSN

0006-2960

Authors

Chao, Alex
Burley, Kalistyn H
Sieminski, Paul J
et al.

Publication Date

2019-11-19

DOI

10.1021/acs.biochem.9b00726

Peer reviewed

HHS Public Access

Author manuscript

Biochemistry. Author manuscript; available in PMC 2020 September 19.

Published in final edited form as:

Biochemistry. 2019 November 19; 58(46): 4610–4620. doi:10.1021/acs.biochem.9b00726.

The structure of a *Mycobacterium tuberculosis* heme-degrading protein, MhuD, variant in complex with its product

Alex Chao[1,‡], **Kalistyn H. Burley**[2,‡], **Paul J. Sieminski**[1], **Rodger de Miranda**[1], **Xiaorui Chen**[1], **David L. Mobley**[2,3], **Celia W. Goulding**[1,2,*]

[1]Department of Molecular Biology & Biochemistry, University of California Irvine, Irvine, CA 92697

[2]Pharmaceutical Sciences, University of California Irvine, Irvine, CA 92697

[3]Chemistry, University of California Irvine, Irvine, CA 92697

Abstract

Mycobacterium tuberculosis (Mtb), the causative agent of tuberculosis, requires iron for survival. In Mtb, MhuD is the cytosolic protein that degrades imported heme. MhuD is distinct, both in sequence and structure, from canonical heme oxygenases (HOs) but homologous with IsdG-type proteins. Canonical HO is found mainly in eukaryotes, while IsdG-type proteins are predominantly found in prokaryotes including pathogens. While there are several published structures of MhuD and other IsdG-type proteins in complex with heme substrate, no structures have been reported of IsdG-type proteins in complex with product, unlike HOs. We recently showed that the Mtb variant MhuD-R26S produces biliverdin IXα (αBV) rather than the wild-type mycobilin isomers as product. Given that mycobilin and other IsdG-type protein products like staphylobilin are difficult to isolate in quantities sufficient for structure determination, here we use the MhuD-R26S variant and its product αBV as a proxy to study the IsdG-type protein/product complex. First we show that αBV has nanomolar affinity for MhuD and the R26S variant. Second we determined the MhuD-R26S-αBV complex structure to 2.5 Å, which reveals two notable features (1) two αBV molecules bound per active site and (2) a novel α-helix (α3) unobserved in previous MhuD-heme structures. Finally, through molecular dynamics simulations we show that α3 is stable with the proximal αBV alone. With MhuD's high affinity for product along with observed structural and electrostatic changes that accompany substrate turnover suggest that there may be an unidentified class of proteins responsible for product extraction from MhuD and other IsdG-type proteins.

Graphical Abstract

*Corresponding Author: celia.goulding@uci.edu.
‡Contributed Equally

The authors declare no competing financial interests.

Accession IDs
hHO-1 P09601
HmuO Q54AI1
MhuD P9WKH3
IsdG Q7A649
IsdI Q7A827
Coordinates and structure factors have been deposited in the Protein Data Bank with a PDB ID: 6PLE.

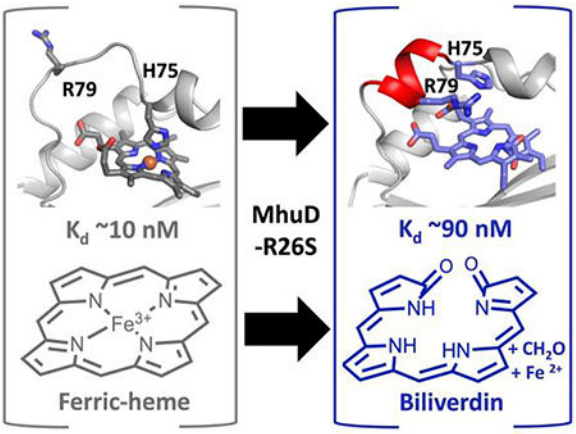

Keywords

Heme degradation; *Mycobacterium tuberculosis*; mycobilin; biliverdin; iron

Introduction

Heme degradation is critical for a variety of biological functions, including iron re-utilization, cell signaling, and antioxidant defense[1–3]. The well-studied canonical heme oxygenase (HO), human HO (hHO-1), catalyzes the oxidative cleavage of heme to release biliverdin IXα (αBV, Figure 1A), ferrous iron, and carbon monoxide (CO)[4–6]. HO homologs are also present in eukaryotes and have been found in some prokaryotes including the pathogens: *Corynebacterium diphtheriae*, *Pseudomonas aeruginosa*, and *Neisseria meningitidis*[7–11]. In eukaryotes, the HO reaction is coupled with the conversion of biliverdin (BV) to bilirubin by biliverdin reductase (BVR)[12]. After conjugation of bilirubin with glucuronic acid, bilirubin is excreted[13]. The fate of HO-produced BV in prokaryotes has not been well studied thus far; although in *P. aeruginosa*, heme is degraded by a HO homolog, HemO, and the BV by-product is excreted, without further reduction, through an unknown[14].

Iron surface determinan*t* G (IsdG)-type proteins, found mainly in bacteria, comprise another heme-degrading protein family distinct from canonical HOs, in both sequence and structure[15–17]. *Staphylococcus aureus* IsdG and IsdI were the first members characterized[16,17], and instead of degrading heme to BV, iron, and CO, these enzymes cleave and oxidize heme at the β- and δ-meso carbon sites to produce staphylobilin isomers (Figure 1A), free iron, and formaldehyde[18,19]. Other IsdG-type enzymes include MhuD from *Mycobacterium tuberculosis* (Mtb) and LFO1 from eukaryotic *Chlamydomonas reinhardtii*, which also degrade heme into unique products[15,20]. While the product(s) of LFO1 heme degradation are yet-to-be-determined[20], MhuD degrades heme into iron and mycobilin isomers (Figure 1A)[21]. Like staphylobilins, the mycobilin isomers are also oxidized at the β- or δ-meso carbons; however cleavage occurs at the α-meso carbon with no observed loss of a C1-product[21]. The lack of C1-product may be physiologically important, as the CO by-product of hHO-1 triggers the transition of Mtb from its active to latent state[21]. Unlike HO-

produced BV, the fate of the IsdG-type protein heme degradation tetrapyrrole products, like staphylobilin and mycobilin, is unknown; however they may have antioxidant properties similar to BV[22].

The structures of HO and IsdG-type proteins are distinct; HOs are predominately monomeric, comprised of a α-helical domain[23], while IsdG-type proteins consist of a homodimeric β-barrel decorated with two α-helices from each subunit[17]. Unsurprisingly, the two distinct classes of heme-degrading enzymes utilize different mechanisms to degrade heme[24]. Although heme is coordinated by a proximal His residue in both HO and IsdG-type enzymes, the heme molecule in HOs is near-planar, while the heme is ruffled for IsdG-type proteins[17,23]. Furthermore, HOs have a distal pocket with a network of ordered water molecules, which facilitates the three consecutive monooxygenase steps required for heme degradation[6]. In contrast, the distal heme pocket is quite hydrophobic for IsdG-type proteins, with only one or two ordered waters observed in the proximal pocket[17,25]. In MhuD, it has been proposed that the hydrophobic pocket and the ruffled heme both contribute to the sequential monooxygenase and dioxygenase steps required for MhuD to degrade heme[24].

The structures of both human and *C. diphtheriae* HO complexed with αBV illustrate that the HO heme degradation reaction is coupled with a conformational change from a ‘closed ‘to ‘open’ state[26,27]. In both the eukaryotic and prokaryotic HO structures, the open-product bound state results from relaxation of the distal and proximal α-helices, and a rotation of the catalytic His side-chain out of the active site pocket, as it is no longer coordinated to heme-iron[26,27]. This structural shift suggests that a degree of protein flexibility is necessary amongst the HO homologs to facilitate catalysis. Structures of apo and monoheme bound forms of IsdG-type proteins reveal an analogous conformational change in the catalytic His residue, as it is absent or disordered in the apo structures; however the ordering of the elongated L2 loop region upon heme binding results in a much more drastic conformational shift compared with those of the HOs (apo-MhuD; Protein Data Bank (PDB) ID: 5UQ4)[17,25,28]. Furthermore unlike other IsdG-type proteins studied to date, MhuD is exceptionally flexible with its active site capable of accommodating two molecules of heme, resulting in protein inactivation[15,25]. The biological significance of this conformational plasticity and its role in product turnover is not well understood as there is no structure of an IsdG-type enzyme in its product-bound form.

The structure of an IsdG-type protein in complex with its heme degradation product would further our understanding of the mechanism of action of this protein family. Unfortunately, staphylobilin and mycobilin products of IsdG-type proteins are difficult to purify[19,21], which has presumably hindered the structural determination of the product-bound form. Recently, we demonstrated that a MhuD variant, MhuD-Arg26Ser (Figure 1B), upon heme degradation produces αBV, formaldehyde, and iron[29]. In this current study, we determine the affinity of wild-type (WT) MhuD and the MhuD-R26S variant to both heme and αBV, and show they both bind heme and αBV in the nanomolar range. This high affinity to αBV allows the utilization of the MhuD-R26S variant as a proxy to study IsdG-type proteins in complex with product. Upon solving the crystal structure of the MhuD-R26S-αBV complex, we observed the formation of a novel secondary structural element unseen in the other heme-bound MhuD structures, and its implications will be discussed further.

Methods

Fluorescence-detection of ligand binding

Fluorescence-detected titrations of heme and αBV were carried out using a previously described protocol[30]. Stock solutions of MhuD (80 nM), heme (8 μM), and αBV (8 μM) were prepared in 50 mM Tris/HCl pH 7.4, 150 mM NaCl. Heme or αBV was titrated and gently mixed in 16 nM or 32 nM increments into MhuD-WT or MhuD-R26S. Following a 1-min incubation, fluorescence emission spectra were acquired between 320 to 500 nm on a Hitachi F-4500 Fluorescence Spectrophotometer through excitation at 285 nm with the following parameters: 1/3 nm step size, scan speed of 240 nm/min, PMT voltage of 700 V, and slit widths at 10 nm (MhuD WT) and 20 nm (MhuD-R26S).

Fluorescence emission spectral analysis

Results from the fluorescence-based assay were fit to Eqn. 1 derived from Conger et el[30, 31], to determine the equilibrium dissociation-constant (K_d) of heme or αBV with MhuD and its mutants.

$$F = \frac{([MhuD] + [ligand] + K_d) - \sqrt{([MhuD] + [ligand] + K_d)^2 - 4[MhuD][Heme]}}{2} \times \left(\frac{F_{min} - F_{max}}{[MhuD]}\right) + F_{max} \quad \text{Eqn. 1}$$

In Eqn. 1, [MhuD] is the total concentration of MhuD or mutant MhuD, [ligand] is the total concentration of heme or αBV, F_{max} is the emission intensity without ligand, and F_{min} is the emission intensity for fully ligand-bound MhuD. Fitting of the fluorescence emission intensity at 340 nm for K_d determination was performed using Origin 2018.

Expression and purification of Mtb MhuD and the R26S variant

WT MhuD and the R26S variant were purified as previously reported[15,29]. In brief, *E. coli* B21-Gold (DE3) cells transformed with pET22b-MhuD plasmid were grown in LB medium containing 50 μg/mL ampicillin at 37°C. Overexpression was induced at OD_{600} of ~ 0.6 using 1 mM IPTG. The cells were harvested 4 hours post induction and resuspended in lysis buffer (50 mM Tris/HCl pH 7.4, 350 mM NaCl and 10 mM imidazole). Cells were lysed via sonication and the resulting lysate was centrifuged at 14,000 rpm. The cell supernatant was loaded onto a Ni^{2+}-charged HiTrap chelating column (5 mL) and washed with lysis buffer. Bound protein was eluted from the column with increasing concentrations of imidazole. Next, MhuD, which elutes at 50 and 100 mM imidazole, was concentrated (Amicon, 5 kDa molecular mass cutoff) and was further purified on a S75 gel filtration column in 20 mM Tris/HCl pH 8, and 10 mM NaCl. A final purification step was performed on an ion-exchange column (HiTrap Q HP, 5 mL) with MhuD eluting at 150 mM NaCl.

Crystallization of MhuD-R26S-αBV complex

To prepare an αBV solution, approximately 2 mg of αBV hydrochloride (SigmaAldrich) was dissolved in 500 μL 0.1 M NaOH followed by 500 μL 1 M Tris/HCl pH 7.4 before

dilution into 50 mM Tris/HCl pH 7.4, 150 mM NaCl. A ferric chloride solution was prepared by dissolving 27.3 mg of ferric chloride hexahydrate (SigmaAldrich) in 10 mL water. A 1.3 fold excess of a 1:1 molar ratio solution of αBV and ferric chloride was gradually added to 100 μM apo-MhuD R26S and incubated overnight at 4°C before being concentrated to 10 mg/mL (Lowry assay)[32]. Light blue crystals appeared in 0.1 M HEPES pH 6.5, 4.6 M NaCl, 30 mM glycyl-glycyl-glycine after 2 days. The crystals were flash frozen in 100% NVH oil and a data set to 1.9 Å was collected at 70K. The collected data was indexed, integrated, and reduced using iMOSFLM[33]. Due to the extremely high degree of anisotropy at higher resolution in the a* direction (http://services.mbi.ucla.edu/anisoscale), the data was cut off at 2.5 Å. Initial phase determination was carried out using Phaser in the PHENIX suite[34] using WT MhuD-heme-CN structure as a search model (PDB ID 4NL5)[25]. αBV molecules were positioned into appropriate positive electron density in the vicinity of the active site, and the structure was refined using phenix.refine[34]. For each monomer, the electron density of the loop region between Ala24 to Asn32 is poorly defined and residues His25-Val30 were modeled as alanines. The only Ramanchandran outliers are Val30 modeled as Ala in both Chain A and B, which are in this poorly defined region of electron density.

Molecular dynamics (MD) simulations

Input files for the MhuD^{4NL5}-heme and MhuD^{4NL5}-αBV simulations were prepared using the structure of dimeric MhuD-heme-CN with the cyano groups removed (PDB ID: 4NL5). For the MhuD-αBV complex, input files were prepared from the MhuD-R26S-αBV structure, wherein the R26S mutation was reversed and just one αBV (proximal) was retained per active site. All crystallographic waters were removed with the exception of the ordered waters in the active site of MhuD^{4NL5} (HOH numbers: 313, 325, 349). Hydrogen atoms were added to the system using pdb4amber from AmberTools15 with default protonation states[35]. For simulations of MhuD^{4NL5}-αBV, each αBV was manually docked to mimic the approximate orientation and position of the proximal αBV from the MhuD-R26S-αBV structure. αBV was parameterized using antechamber from AmberTools15[35] with GAFF version 1.7 and AM1-BCC charges. The ligated His75-Fe-heme ligand was parameterized according to previously published Density Functional Theory calculations[36]. Missing atoms for each structure were added using tleap in AmberTools15[35], and parameterized using ff99SBildn[37]. Each system was explicitly solvated in tleap with a 10 Å rectangular box of TIP3P water, extending from the surface of the protein to the box edge, and sodium ions were added to neutralize the charge of the system.

Minimization proceeded using *sander* from Amber14[35] with steepest descents running for 20,000 timesteps of 2 fs each, followed by heating from 100 K to 300 K with constant volume for 25,000 timesteps of 2 fs. Equilibration continued using *sander* for 500,000 timesteps of 2 fs under constant pressure with positional restraints initially applied on all non-water atoms at 50 kcal/mol/Å^2 and progressively lifted in increments of 5 kcal/mol/Å^2 over ten 50,000 step segments. The resulting topology and coordinate files for each system were used as inputs for MD simulations. Production simulations were executed in OpenMM 7.1.0[38] using a Langevin integrator with a 2 fs timestep and a friction coefficient of 10/ps. For each of the three systems, five independent simulations of 100 ns each were initiated

with randomized velocities. Among the five simulations, one simulation was restarted for each system for an additional 500 ns, bringing the total simulation time to 1 μs/system.

MD analysis

Distances and secondary structure assignments were computed using MDTraj[39]. For analysis, each monomer of MhuD was treated independently with the assumption that long-range interactions between each subunit are negligible for the time scales simulated here. To analyze the orientation of His75 during simulations, two orientations were defined: 1) *Active Site* – side chain pointing into binding pocket, towards the center of the tetrapyrrole, and 2) *Solvent Exposed* – side chain flipped away from the binding pocket, as in the MhuD-αBV structure (see Figure 4Bi). To assign these positions, we computed the distance between the ε nitrogen atom (furthest from the backbone) on His75 and the nitrogen atom located between the α and β carbons on either αBV or heme. If the distance was less than 6 Å, the His75 residue was classified as being oriented in the *Active Site* position; otherwise the position was classified as *Solvent Exposed*.

For the Arg79 positional analysis, we identified four positions; 1) *Active site* – Arg79 directed into the binding pocket interacting with the ligand, 2) *Helix 1* – Arg79 side-chain interacting with residues on α-helix-1 (i.e residues 16–25) of MhuD, 3) *Helix 2* – Arg79 side-chain interacting with residues on α-helix-2 (residues 60–75), and 4) *Solvent Exposed* – Arg79 side-chain oriented into the surrounding solvent. To analyze the Arg79 in our simulations, position assignments were defined as follows: 1) *Active Site* – guanidinium carbon of Arg79 side-chain (CZ) within 4.5 Å of either terminal carbon on the propionate groups of the heme or αBV ligands. 2) *Helix 1* - Arg79 CZ atom within 6 Å of Glu16 α carbon 3) *Helix 2* – Arg79 CZ atom within 6 Å of His75 or Ile72 backbone oxygen and more than 4.5 Å from terminal carbons on the propionate groups of the heme or αBV ligands. 4) *Solvent Exposed* – Any position of Arg79 falling outside the description of positions 1–3.

Results

Affinity of substrate and product to MhuD

Previously, the affinity (K_d) of WT-MhuD for heme was measured to be ~6 nM[30]; empirically it has been observed that MhuD also has a high affinity for its product, as isolation of MhuD mycobilin products requires iron chelation followed by protein denaturation[21,29]. Recently, we demonstrated that the MhuD-R26S variant degrades heme to produce αBV as its predominate tetrapyrrole product rather than the WT mycobilin isomers[21,29]. As it is difficult to isolate large quantities of mycobilin, in this study the MhuD-R26S variant and its αBV product is utilized as a model system to study IsdG-type proteins in complex with product. First, we determined the affinities of heme and αBV to both WT-MhuD and the MhuD-R26S variant using a previously described fluorescence-based assay (Figure 2)[30]. The affinities of WT-MhuD and MhuD-R26S for heme are ~6nM and ~9nM, respectively (Table 1). The reduced affinity of heme to the MhuD-R26S variant compared to WT-MhuD may be due to the loss of the water-mediated interaction of Arg26 with the heme propionate (Figure 1B) when Arg26 is mutated to Ser. By comparison, both

WT-MhuD and MhuD-R26S have weaker affinity for αBV of ~36 nM and ~92 nM, respectively (Table 1). However, we observe the same trend as for heme, where WT-MhuD binds αBV with a higher affinity than the MhuD-R26S variant (even though the WT product of MhuD is mycobilin rather than αBV), which suggests that the Arg26 residue may form contacts with the tetrapyrrole product.

The structure of the MhuD-R26S-αBV complex

To investigate the structural impacts on MhuD arising from heme degradation into product, we turned our attention to structure determination of MhuD-R26S in complex with αBV. The MhuD-R26S-αBV complex crystallized in the presence of ferric chloride, and light blue crystals appeared in 0.1 HEPES pH 6.5, 4.6 M NaCl and 30 mM glycyl-glycyl-glycine after 2 days. The structure of MhuD-R26S-αBV was solved to 2.5 Å resolution with a final R/R_{free} of 23.2/28.5 (Table 2). The asymmetric unit contains five stacked αBV molecules that link individual subunits from two adjacent, biologically relevant homodimers (Figure 3A). The monomers in the asymmetric unit, each in complex with two αBV molecules, superimpose with a root-mean-square deviation (RMSD) of 0.2 Å, and the five stacked αBV molecules model well into the electron density (Figure S1). The biologically relevant MhuD-R26S homodimeric structure is observed in the crystallographic 2-fold symmetry (Figure 3B), similar to apo- and heme-bound MhuD homodimer structures (apo-MhuD; PDB code: 5UQ4)[15,25]. By size exclusion chromatography, the MhuD-R26S-αBV complex was confirmed to be a dimer in solution, Figure S2.

The MhuD-R26S-αBV homodimeric structure is similar to that of the MhuD-heme-CN and MhuD-diheme structures[15,25], where each subunit forms a ferredoxin-like fold. To form the homodimer, each polypeptide chain donates four β-strands to form the eight-stranded antiparallel β-barrel. Additionally, each monomer has three α-helices together with two flexible loop regions; the first loop connects α-helix-1 to β-strand-2 and the second connects α-helix-3 to β-strand-4 (Figure 3B). It should be noted that the overall topology of the MhuD-R26S-αBV monomer differs from those of the apo-MhuD and MhuD-heme-CN structures[25]. Within the MhuD-R26S-αBV structure, there is an additional short α-helix-3 formed by residues Ala76-Asn81, which was not observed in the monoheme, diheme and apo-MhuD structures[15,25], and thus the latter structures have a slightly longer extended L2 loop region. There are also other subtle conformational changes that will be discussed later.

αBV Binding to MhuD

Each MhuD-R26S active site binds two molecules of αBV (Figures 3B). The solvent-protected or proximal αBV interacts with both MhuD and the distal αBV, and the distal αBV also interacts with MhuD. The proximal αBV forms five electrostatic and eleven hydrophobic interactions with MhuD residues. The αBV propionate-6 carboxylate group hydrogen-bonds (H-bonds) with the backbone amides of Val83 and Ala84 (2.9 and 2.6 Å, respectively), and forms a salt-bridge with the NH1 group of Arg22 (2.7 Å). Additionally, Trp66 NE1 H-bonds (2.7 Å) with the A-ring lactam oxygen (=O), and Asn7 ND2 H-bonds (2.7 Å) to the D-ring lactam oxygen (Figure 3C). The tetrapyrrole plane of the distal αBV is nearly parallel to that of the proximal αBV.

The proximal and distal αBV molecules interact through hydrophobic and van der Waals interactions only. The distal αBV is rotated ~205° and flipped ~180° with respect to the αBV tetrapyrrole plane, and the distal αBV tetrapyrrole plane is positioned ~3.4 Å above and translated ~5.0 Å relative to the proximal αBV plane. Consequently, the C-ring of the distal αBV is partially placed over the A-ring of the proximal αBV resulting in the distal αBV being more solvent exposed than the proximal one (Figure 3D). The proximal αBV forms five H-bonds with MhuD whereas the distal αBV forms only three and has fewer hydrophobic interactions with MhuD than the proximal αBV (Figure 3D). The A-ring lactam oxygen of the distal αBV H-bonds with Arg79 NE and NH1 (3.1 and 2.7 Å, respectively), and the distal αBV propionate-6 H-bonds to the Leu89 amide group (3.2 Å).

Along with the proximal and distal αBV subunits, there is a third 'bridging' αBV, which connects the two symmetrical subunits each bound to two αBV molecules (Figure 3A). The third 'bridging' αBV is parallel to the tetrapyrrole plane of the flanking distal αBV molecule from each subunit and is separated by ~3.8 Å from each distal αBV. Additionally, the bridging αBV is rotated ~90° and translated ~2.5 Å with respect to the distal αBV molecules. The bridging αBV interacts with the distal αBVs by hydrophobic and van der Waals interactions, and also forms one H-bond to each, where the bridging αBV ring-D/A lactam oxygen H-bonds to the ring-A/D pyrrole nitrogen of the distal αBVs (2.8 Å and 3.3 Å), respectively. Finally, the bridging αBV forms a H-bond to each MhuD subunit, ring-A/D lactam oxygen H-bonds with Arg79 NH2 group on respective subunits (3.0 and 2.6 Å, respectively).

Comparison of MhuD substrate and product bound structures

There are several distinct structural differences between the inactive substrate-bound (MhuD-heme-CN)[25] and product-bound (MhuD-R26S-αBV) MhuD structures, despite an RMSD of 1.1 Å (Figure 4A). The most notable difference between the two structures is within α-helix-2 and the sequential loop region L2. In MhuD–heme–CN, the α-helix-2 is kinked after residue Asn68 and terminates at His75, where this region in the MhuD-R26S-αBV structure has a looser helical geometry. This kinked helical region in the MhuD-heme-CN structure positions the catalytic His75 within the active site so it coordinates with heme-iron. However, in MhuD-R26S-αBV, His75 flips out of the active site (90° rotation and translation of 2.8 Å of the Cα, Figure 4Bi) and is stabilized by a H-bond between the His75 imidazole nitrogen to the backbone carbonyl of Ala27 (3.2 Å). In combination with the slight unraveling of the C-terminus of α-helix-2 in MhuD-R26S-αBV, the extended loop L2 region has an additional α-helix (α3, Ala76-Asn81) as compared to MhuD-heme-CN[25] (Figure 4A). Within the L2 loop region of MhuD-heme-CN, both His78 and Arg79 are solvent-exposed with no observable electron density for the Arg79 side-chain. In contrast, in MhuD-R26S-αBV, Arg79 is located in α-helix-3, and its side-chain is positioned towards the active site and is stabilized by a H-bond between its NH1 group with the backbone carbonyl of Ile72 (3.1 Å) (Figure 4Bii); notably His78 is still solvent-exposed and weakly stabilized by a cation-π interaction between its imidazole side-chain and Arg22 (3.7 Å).

Another minor structural difference between substrate and product bound MhuD complexes is the unraveling of the C-terminal α-helix-1 in MhuD-R26S-αBV compared to MhuD-

heme-CN. Arg26 is situated in this location and participates in a water-mediated H-bond with one of the heme propionates in the MhuD-heme-CN structure[25] (Figures 1B & 4A). Within the MhuD-R26S-αBV structure, this region is no longer helical. Thus, this observed unraveling of α-helix-1 may be the result of the Arg26Ser mutation, however, this conformational change ensures that the backbone carbonyl group of the subsequent residue, Ala27, is in H-bonding distance of the imidazole nitrogen of His75, to stabilize the flipped out His75 in the MhuD-R26S-αBV structure[21].

The conformational change from going from substrate to product bound also alters the active site pocket volume and the electrostatic potential of the molecular surface (Figures 4C & 4D). The active site volume increases dramatically from heme bound to that of αBV, from 188 to 354 $Å^3$, calculated utilizing CASTp[40]. In conjunction with the increased active site volume, the molecular surface region surrounding the active site and the L2 loop region undergoes an electrostatic potential change. The MhuD molecular surface surrounding one side of the exposed active site is positively and negatively charged in the presence of heme (Figure 4C), whereas in the presence of αBV it becomes more hydrophobic and negatively charged with a positively charged bridge capping the active site (Figure 4D). Furthermore, when rotated 90° about the y-axis, there is altered molecular surface electrostatics from positively charged and hydrophobic to predominately negatively charged in the presence of heme and αBV, respectively (Figures 4C & 4D, right panels).

MD Simulations

MD simulations were performed to gain further insight into the protein conformational changes associated with heme and αBV binding. In particular, we wanted to evaluate the *in silico* stability of the MhuD α-helix-3 (Ala76-Asn81) in the presence of proximal αBV alone. MD simulations were set up using the biological dimer of the MhuD-R26S-αBV structure with the R26S mutation modeled as WT Arg26 and only the proximal αBVs retained. Heretofore, we refer to this system in our MD analysis as MhuD-αBV. Over the 1 μs of combined simulation time, including a continuous 600 ns simulation, the α-helix-3 persisted in MhuD-αBV for over 70% of the run, suggesting that the α-helix-3 is stable when there is just one αBV molecule present per active site. Interestingly, we also observe some helix formation within the L1 loop region, an otherwise highly flexible region of the protein (Figure 5).

To test if the α-helix-3 forms during turnover from heme to product, two more sets of simulations were carried out. The first contained the MhuD-heme-CN structure without the cyano group ($MhuD^{4NL5}$-heme) while the second was comprised of the $MhuD^{4NL5}$ protein structure with αBV docked in place of heme to give $MhuD^{4NL5}$-αBV. For this system, the αBVs were manually docked in the orientation and position of the proximal αBV from the MhuD-R26S-αBV structure. As with the MhuD-αBV simulations, the $MhuD^{4NL5}$-αBV and $MhuD^{4NL5}$-heme simulations each ran for a total of 1 μs. Although the two αBV MD systems (MhuD-αBV and $MhuD^{4NL5}$-αBV) are identical in composition, they have distinct initial positions and velocities; MhuD-αBV simulations start from the coordinates of the αBV-bound crystal structure while $MhuD^{4NL5}$-αBV simulations start from those of the heme-bound structure. Given sufficient simulation time, the dynamics of these two systems

should eventually converge. While we did not reach convergence, it is compelling that we see some *de novo* formation of the α-helix-3 in our simulation of MhuD^{4NL5}-αBV (Figure 5), suggesting that it is a relevant structural motif that forms in the presence of αBV. We speculate that the α-helix-3 may be further stabilized by contact of MhuD with accessory proteins. This α-helix-3 is also transiently observed in the MhuD^{4NL5}-heme simulation (Figure 5); however its occurrence is less frequent compared to MhuD^{4NL5}-αBV. In addition, the binding mode of the modeled αBV, in both the MhuD-αBV and MhuD^{4NL5}-αBV simulations, is stable and consistent with the hypothesis that the proximal αBV in the MhuD-R26S-αBV structure mimics the orientation of the WT MhuD product.

We also sought to evaluate whether the 90° rotation of the catalytic His75 side chain away from the active site, as observed in the MhuD-αBV structure (Figures 4Bi & 6), is facilitated by substrate turnover to αBV. In the MhuD-αBV simulations, His75 residue remains in the "flipped out" or solvent exposed orientation (Figure 6B) while in the MhuD^{4NL5}-heme simulations, it is ligated to the heme-iron atom and thus remains tethered to the active site. For MhuD^{4NL5}-αBV, the His75 alternates between the two orientations (Figure 6C), as shown in Figures 6A & 6B. The solvent exposed position may be further stabilized in the MhuD^{4NL5}-αBV simulations after extended simulation time and upon full formation of the α-helix-3, as observed in the MhuD-αBV structure, where the Arg79 side-chain forms a hydrogen bond with the backbone carbonyl of Ile72 (Figure 4Bii).

Because the Arg79 side-chain is unresolved in the MhuD^{4NL5}-heme structure but stabilized in the MhuD-αBV structure, we were also interested in exploring its dynamics in the presence of heme versus αBV. Upon inspection of the MhuD^{4NL5}-heme simulations, four classifications of Arg79 positions were identified: helix 1 and helix 2 (interacting with residues on α-helix-1 or on α-helix-2), active site (interacting with heme or αBV) and solvent exposed (Figures 7A–D). In the MhuD^{4NL5}-heme simulations, the varied distribution of the Arg79 positions mirrors its disorder in the crystal structure (Figure 7E). Unexpectedly, we found at times that the Arg79 forms H-bonds with the propionate groups of the heme; in fact, in the extended 600ns simulation of MhuD^{4NL5}-heme, the Arg79 residue for one MhuD subunit flipped into the active site and remained coordinated to the heme ligand for over 90% of the simulation (data not shown). In simulations with αBV, Arg79 interacts with residues on helix 2 or becomes solvent exposed. Consistent with the MhuD-αBV structure, the predominant state in the MhuD-αBV simulations shows it interacting with helix 2 (Figure 7F). In our MhuD^{4NL5}-αBV simulation, the favored state is solvent exposed (Figure 7G), but we suspect the interaction of Arg79 with helix 2 may be further stabilized upon full formation of α-helix-3. Given that we only observe Arg79 interacting with the ligand propionate groups in simulations where His75 is oriented into the active site, we hypothesize that Arg79 plays a critical role in promoting catalysis (when heme is present) and facilitating product egress (via formation of α-helix-3).

Together these results suggest that in the MhuD-R26S-αBV structure we are (1) observing the proximal αBV in an orientation and location equivalent to the turnover product, (2) that the additional α-helix-3 present in the MhuD-product complex is not a crystallographic artifact and, (3) the 90° rotation of His75 out of the active site is consistent with substrate turnover. In addition, the simulations implicate Arg79 as a putative catalytic residue that also

facilitates formation of α-helix-3 upon MhuD turnover—an observation that warrants further biochemical investigation

Proximal αBV is representative of the MhuD physiological product

Within the MhuD-R26S-αBV structure, the orientation of the proximal αBV is representative of the MhuD physiological product, mycobilin. The proximal αBV adopts a similar orientation as heme in the active site of the MhuD-heme-CN structure (Figures 4A–B)[25], however αBV is rotated approximately 20° about the plane compared to heme-CN and the tetrapyrrole ring structure of αBV is considerably more twisted compared to heme. The reduced affinity of αBV to the MhuD-R26S variant, compared to WT-MhuD, supports that the proximal αBV in the MhuD-R26S-αBV structure adopts a similar orientation as the WT MhuD product. As observed for heme-bound MhuD, where Arg26 interacts with the heme propionate, Arg26 likely forms a non-covalent interaction with the tetrapyrrole product as well; thus, after catalysis, one would expect that location of the product would mirror that of substrate heme, as we observe for the proximal αBV. Additionally, the overall conformation of MhuD proximal αBV is similar to the αBV product of *C. diphtheriae* HmuO (PDB 4GPC)[27], representative of the all-Z-all-syn type BV conformation. However, in another structure of hHO-1 in complex with αBV (PDB 1S8C)[26], the αBV occupies an internal cavity adjacent to the active site and exhibits a more linear extended conformation. This was proposed to be the route of αBV dissociation from hHO-1 in the absence of BVR[26]. As αBV is bound tightly to MhuD, we did not anticipate that we would observe a partially dissociated product conformation or location, as seen in the hHO-1 structure. Furthermore, in the MD simulations of the proximal αBV alone in the MhuD-R26S-αBV structure, αBV remains in the same relative location and orientation also supporting that this is the correct product orientation. Together these observations suggest that the proximal αBV within MhuD-R26S-αBV structure is the physiological orientation of the MhuD tetrapyrrole product, mycobilin, within the active site.

Discussion

Within the PDB there is only one other protein structure with a strikingly similar αBV stacking conformation in its active site, a BVR from cyanobacteria[41]. As with the MhuD-R26S-αBV structure, the BVR-αBV structure has offset nearly parallel tetrapyrrole planes stacked at van der Waals distance and although the proximal and distal αBV molecules in MhuD have no inter-molecular H-bonds, the BVR αBV molecules form an intermolecular H-bond between the lactam oxygen and pyrrole nitrogen, as observed between the distal and ‘bridging’ αBV molecules in the MhuD-R26S-αBV asymmetric unit (Figure 3A).

Tetrapyrrole stacking is sometimes important for enzyme activity, however it has also been observed that heme-heme stacking can be the product of crystallization. Heme stacking has previously been shown to be involved in protein electron transfer reactions; for example, NapB, a cytochrome subunit of nitrate reductase, requires two stacked heme molecules for electron transfer[42]. More recently it was demonstrated that the cyanobacterial BVR required two stacked BVs to reduce BV to bilirubin[41] by an unprecedented mechanism. In contrast, MhuD can also accommodate two stacked heme molecules per active site, although this

renders the enzyme inactive[15]. Tetrapyrrole stacking at the crystallographic interface is not unprecedented, as observed in the structures of MhuD-diheme[15], and the ChaN-heme[43], an iron-regulated lipoprotein implicated in heme acquisition in *Campylobacter jejuni*. As MhuD is known to be active only in its monoheme form[15], and thus only produces one molecule of product per active site, we hypothesize that the proximal αBV is in the correct orientation of the MhuD tetrapyrrole product; consequently, the three additional stacked αBV molecules adjoining the two active sites of adjacent MhuD monomers are likely a product of crystallization.

The conformational changes between the MhuD substrate and product bound structures, while relatively subtle based on RMSD, are significant compared to those of canonical HOs. These differences are borne out in the fluctuation of the active site volume (Figure S3A). The structures of *C. diphtheriae* HO (HmuO) in its substrate- and product-bound form (PDB 1IW0, 4GPC) show some shifting and unwinding of the active site proximal and distal helices[27], while the change in the active site pocket volume is trivial (from ~250 $Å^3$ to ~260 $Å^3$)[40]. By comparison, MhuD demonstrates much greater conformational versatility. When MhuD binds one heme molecule in its active form, the C-terminal of α-helix-1 unravels to accommodate the heme molecule and the C-terminal region of α-helix-2 extends to all the catalytically essential His75 to coordinate heme-iron, resulting in a kinked α-helix-2. The MhuD-monoheme complex can also bind another molecule of heme resulting in its diheme inactive form, whereby the kinked α-helix-2 is now extended and His75 binds to heme-iron of the solvent exposed heme molecule, nearly tripling the volume of the active site from ~190 $Å^3$ to ~530 $Å^3$ compared to the monoheme structure[40]. Alternatively, when MhuD-monoheme turns over in the presence of an electron source, it forms the MhuD-product structure, which leads to the further unraveling of the C-terminal of α-helix-1 and the kinked α-helix-2 along with the formation of α-helix-3. With the transformation of substrate to product, the active site of MhuD doubles in volume, from ~190 $Å^3$ to ~360 $Å^3$[3, 40]. The four different conformational states of MhuD highlight this protein's inherent flexibility (Figure S3B), which may be harnessed to produce MhuD inhibitors.

Little is known about the fate of IsdG-like protein products; but removal of their tetrapyrrole products requires protein denaturation[19,21]. Indeed, our previous and current work suggest that both MhuD substrate and product bind in the low nanomolar range and therefore the displacement of product by substrate would only occur at high heme concentrations *in vivo*[30]. We propose three possible mechanisms of MhuD product release; (1) a dramatic conformational change would reduce product affinity and result in dissociation, (2) IsdG-type proteins are 'suicide' proteins that after one turnover require degradation or (3) an accessory protein is required for the removal of product from the MhuD active site.

Although MhuD is an inherently flexible protein, as described above, its high affinity for tetrapyrroles decreases the likelihood that a conformational change alone would promote product release. Because it has been shown that *S. aureus* IsdG is degraded *in vivo* in its apo form, yet stabilized in the presence of heme[44], it seems unlikely that IsdG-type enzymes are also degraded when bound to product. As the MhuD-R26S-αBV complex structure has a novel structural element and an associated shift in molecular surface electrostatics in comparison to MhuD-monoheme complex, these conformational changes may promote

protein-protein interactions to aid in product removal. Notably, the ^{75}HisXXXArg^{79} motif encompassing the newly formed α-helix-3 is also observed in IsdG-type proteins *S. aureus* IsdG and IsdI (Figure S4). Formation of this helix upon substrate turnover may be a common feature among all IsdG-type proteins that facilitates removal of their tetrapyrrole products, although further work is required to validate this hypothesis.

Protein-protein interaction-induced product removal is reminiscent of human HO-1 BV removal. Human BVR interacts with hHO-1, albeit via a weak interaction, to remove the product BV and further reduce it to bilirubin[45]. In contrast, the well-studied bacterial HO from *P. aeruginosa* excretes BV without further reduction[14]. We hypothesize that a yet-to-be-identified Mtb protein removes product from MhuD and potentially aids in its eventual excretion, as observed in the human HO system. Surprisingly, Mtb has four close homologs of BVR even though Mtb does not have a conventional BV-producing HO enzyme[15]. One of these homologs, Rv2074, has BV reduction activity although its electron donating cofactor is the flavin cofactor F420[46], a deazaflavin cofactor that is a low potential hydride transfer agent[47], rather than flavin mononucleotide (FMN) as observed for eukaryotic BVRs[48]. In contrast, Rv1155 does not readily reduce BV[49]. Consequently, it was proposed that one of the BV inactive Mtb BVRs catabolizes mycobilins. Rv2607 and Rv2991 have not been tested for BVR activity and could also act in MhuD product breakdown[49]. Mtb has both heme and siderophore-mediated iron acquisition systems[50], however *Mycobacterium leprea* only has a heme uptake and catabolism pathway. Furthermore, the *M. leprea* proteome only has the Mtb BVR homologs, Rv1155 and Rv2607, suggesting one of these proteins is perhaps involved in MhuD product removal.

The MhuD-product complex structure has an additional α-helix-3 and an accompanying change in electrostatic surface potential compared to the MhuD-substrate complex[15]. The structure and MD simulations suggest that α-helix-3 forms when His75 is no longer coordinated to the heme-iron and can freely flip out of the binding pocket. Furthermore this new α-helix-3 is stabilized by Arg79 moving into the active site vicinity, whereby Arg79 is a residue previously unresolved in both the heme-bound and apo-MhuD structures[15, 25]. Given our results, the conservation of ^{75}HisXXXArg^{79} in other IsdG-type proteins, and the presence of BVR homologs in MhuD, we hypothesize that α-helix-3 formation may be a common structural feature among all product-bound IsdG-type proteins that facilitates protein-protein interactions in order to promote product egress.

Supplementary Material

Refer to Web version on PubMed Central for supplementary material.

Acknowledgements

We would like to thank Tom Poulos for discussions and critical reading of the manuscript, as well as Dr. Fengyun Ni, Baylor College of Medicine for advice on the more difficult aspects of structure refinement. We thank the Advanced Light Source at Berkeley National Laboratories (ALS) and the Stanford Synchrotron Radiation Lightsource (SSRL) for their invaluable help in data collection, and The Triton Shared Computing Cluster (TCSS) at the San Diego Supercomputing Center (SSDC) for their computing support.

Funding

C.W.G. thanks the National Institutes of Health (NIH) for financial support (P01-AI095208), A.C. thanks the National Science Foundation for predoctoral fellowship support (DGE-1321846), and K.H.B. thanks the NIH for support from a predoctoral training grant (T32GM108561).

References

[1]. Dore S, Takahashi M, Ferris CD, Zakhary R, Hester LD, Guastella D, and Snyder SH (1999) Bilirubin, formed by activation of heme oxygenase-2, protects neurons against oxidative stress injury. Proc. Natl. Acad. Sci. U S A 96, 2445–2450. [PubMed: 10051662]

[2]. Ferris CD, Jaffrey SR, Sawa A, Takahashi M, Brady SD, Barrow RK, Tysoe SA, Wolosker H, Baranano DE, Dore S, Poss KD, and Snyder SH (1999) Haem oxygenase-1 prevents cell death by regulating cellular iron. Nat. Cell. Biol 1, 152–157. [PubMed: 10559901]

[3]. Brouard S, Otterbein LE, Anrather J, Tobiasch E, Bach FH, Choi AM, and Soares MP (2000) Carbon monoxide generated by heme oxygenase 1 suppresses endothelial cell apoptosis. J. Exp. Med 192, 1015–1026. [PubMed: 11015442]

[4]. Tenhunen R, Marver HS, and Schmid R (1969) Microsomal heme oxygenase. Characterization of the enzyme. J. Biol. Chem 244, 6388–6394. [PubMed: 4390967]

[5]. Yoshida T, Noguchi M, and Kikuchi G (1980) Oxygenated form of heme - heme oxygenase complex and requirement for second electron to initiate heme degradation from the oxygenated complex. J. Biol. Chem 255, 4418–4420. [PubMed: 6892813]

[6]. Matsui T, Unno M, and Ikeda-Saito M (2010) Heme oxygenase reveals its strategy for catalyzing three successive oxygenation reactions. Acc. Chem. Res 43, 240–247. [PubMed: 19827796]

[7]. Schmitt MP (1997) Utilization of host iron sources by Corynebacterium diphtheriae: identification of a gene whose product is homologous to eukaryotic heme oxygenases and is required for acquisition of iron from heme and hemoglobin. J. Bacteriol 179, 838–845. [PubMed: 9006041]

[8]. Wilks A, and Schmitt MP (1998) Expression and characterization of a heme oxygenase (Hmu O) from Corynebacterium diphtheriae. Iron acquisition requires oxidative cleavage of the heme macrocycle. J. Biol. Chem 273, 837–841. [PubMed: 9422739]

[9]. Zhu W, Wilks A, and Stojiljkovic I (2000) Degradation of heme in gram-negative bacteria: the product of the hemO gene of Neisseriae is a heme oxygenase. J. Bacteriol 182, 6783–6790. [PubMed: 11073924]

[10]. Ratliff M, Zhu W, Deshmukh R, Wilks A, and Stojiljkovic I (2001) Homologues of neisserial heme oxygenase in gram-negative bacteria: degradation of heme by the product of the pigA gene of Pseudomonas aeruginosa. J. Bacteriol 183, 6394–6403. [PubMed: 11591684]

[11]. Wilks A (2002) Heme oxygenase: evolution, structure, and mechanism. Antioxid. Redox Signal 4, 603–614. [PubMed: 12230872]

[12]. Noguchi M, Yoshida T, and Kikuchi G (1979) Specific requirement of NADPH-cytochrome c reductase for the microsomal heme oxygenase reaction yielding biliverdin IX alpha. FEBS Lett. 98, 281–284. [PubMed: 105935]

[13]. Mantle TJ (2002) Haem degradation in animals and plants, Biochem Soc Trans 30, 630–633. [PubMed: 12196151]

[14]. Barker KD, Barkovits K, and Wilks A (2012) Metabolic flux of extracellular heme uptake in Pseudomonas aeruginosa is driven by the iron-regulated heme oxygenase (HemO). J. Biol. Chem 287, 18342–18350. [PubMed: 22493498]

[15]. Chim N, Iniguez A, Nguyen TQ, and Goulding CW (2010) Unusual diheme conformation of the heme-degrading protein from Mycobacteriuim tuberculosis. J. Mol. Biol 395, 595–608. [PubMed: 19917297]

[16]. Skaar EP, Gaspar AH, and Schneewind O (2004) IsdG and IsdI, heme-degrading enzymes in the cytoplasm of Staphylococcus aureus. J. Biol. Chem 279, 436–443. [PubMed: 14570922]

[17]. Wu R, Skaar EP, Zhang R, Joachimiak G, Gornicki P, Schneewind O, and Joachimiak A (2005) Staphylococcus aureus IsdG and IsdI, heme-degrading enzymes with structural similarity to monooxygenases. J. Biol. Chem 280, 2840–2846. [PubMed: 15520015]

[18]. Matsui T, Nambu S, Ono Y, Goulding CW, Tsumoto K, and Ikeda-Saito M (2013) Heme degradation by Staphylococcus aureus IsdG and IsdI liberates formaldehyde rather than carbon monoxide. Biochemistry 52, 3025–3027. [PubMed: 23600533]

[19]. Reniere ML, Ukpabi GN, Harry SR, Stec DF, Krull R, Wright DW, Bachmann BO, Murphy ME, and Skaar EP (2010) The IsdG-family of haem oxygenases degrades haem to a novel chromophore. Mol. Microbiol 75, 1529–1538. [PubMed: 20180905]

[20]. Lojek LJ, Farrand AJ, Wisecaver JH, Blaby-Haas CE, Michel BW, Merchant SS, Rokas A, and Skaar EP (2017) Chlamydomonas reinhardtii LFO1 Is an IsdG Family Heme Oxygenase. mSphere 2, e00176–17. [PubMed: 28815214]

[21]. Nambu S, Matsui T, Goulding CW, Takahashi S, and Ikeda-Saito M (2013) A new way to degrade heme: the Mycobacterium tuberculosis enzyme MhuD catalyzes heme degradation without generating CO. J. Biol. Chem 288, 10101–10109. [PubMed: 23420845]

[22]. Vanella L, Barbagallo I, Tibullo D, Forte S, Zappala A, and Li Volti G (2016) The non-canonical functions of the heme oxygenases. Oncotarget 7, 69075–69086. [PubMed: 27626166]

[23]. Schuller DJ, Wilks a., Ortiz de Montellano PR, and Poulos TL (1999) Crystal structure of human heme oxygenase-1. Nat. Struct. Biol 6, 860–867. [PubMed: 10467099]

[24]. Matsui T, Nambu S, Goulding CW, Takahashi S, Fujii H, and Ikeda-Saito M (2016) Unique coupling of mono- and dioxygenase chemistries in a single active site promotes heme degradation. Proc. Natl. Acad. Sci. U S A 113, 3779–3784. [PubMed: 27006503]

[25]. Graves AB, Morse RP, Chao A, Iniguez A, Goulding CW, and Liptak MD (2014) Crystallographic and spectroscopic insights into heme degradation by Mycobacterium tuberculosis MhuD. Inorg. Chem 53, 5931–5940. [PubMed: 24901029]

[26]. Lad L, Friedman J, Li H, Bhaskar B, Ortiz de Montellano PR, and Poulos TL (2004) Crystal structure of human heme oxygenase-1 in a complex with biliverdin. Biochemistry 43, 3793–3801. [PubMed: 15049686]

[27]. Unno M, Ardevol A, Rovira C, and Ikeda-Saito M (2013) Structures of the substrate-free and product-bound forms of HmuO, a heme oxygenase from Corynebacterium diphtheriae: x-ray crystallography and molecular dynamics investigation. J. Biol. Chem 288, 34443–34458. [PubMed: 24106279]

[28]. Lee WC, Reniere ML, Skaar EP, and Murphy ME (2008) Ruffling of metalloporphyrins bound to IsdG and IsdI, two heme-degrading enzymes in Staphylococcus aureus. J. Biol. Chem 283, 30957–30963. [PubMed: 18713745]

[29]. Chao A, and Goulding CW (2019) A Single Mutation in the Mycobacterium tuberculosis Heme-Degrading Protein, MhuD, Results in Different Products. Biochemistry 58, 489–492. [PubMed: 30605595]

[30]. Thakuri B, Graves AB, Chao A, Johansen SL, Goulding CW, and Liptak MD (2018) The affinity of MhuD for heme is consistent with a heme degrading function in vivo. Metallomics 10, 1560–1563. [PubMed: 30239544]

[31]. Conger MA, Pokhrel D, and Liptak MD (2017) Tight binding of heme to Staphylococcus aureus IsdG and IsdI precludes design of a competitive inhibitor. Metallomics 9, 556–563. [PubMed: 28401968]

[32]. Lowry OH, Rosebrough NJ, Farr AL, and Randall RJ (1951) Protein measurement with the Folin phenol reagent. J. Biol. Chem 193, 265–275. [PubMed: 14907713]

[33]. Battye TG, Kontogiannis L, Johnson O, Powell HR, and Leslie AG (2011) iMOSFLM: a new graphical interface for diffraction-image processing with MOSFLM. Acta Crystallogr. D Biol. Crystallogr 67, 271–281. [PubMed: 21460445]

[34]. Adams PD, Afonine PV, Bunkoczi G, Chen VB, Davis IW, Echols N, Headd JJ, Hung LW, Kapral GJ, Grosse-Kunstleve RW, McCoy AJ, Moriarty NW, Oeffner R, Read RJ, Richardson DC, Richardson JS, Terwilliger TC, and Zwart PH (2010) PHENIX: a comprehensive Python-based system for macromolecular structure solution. Acta Crystallogr. D Biol. Crystallogr 66, 213–221. [PubMed: 20124702]

[35]. Case DA, Cerutti DS, Cheatham TE III, Darden TA, Duke RE, Giese TJ, Gohlke H, Goetz AW, Greene D, Homeyer N, Izadi S, Janowski P, Kaus J, A., and Kovalenko TSL, LeGrand S, Li P, Luchko T, Luo R, Madej B, Merz KM, Monard G, Needham P, Nguyen H, Nguyen HT, Omelyan

I, Onufriev A, Roe DR, Roitberg A, Salomon-Ferrer R, Simmerling CL, Smith W, Swails J, Walker RC, Wang J, Wolf RM, Wu X, York DM and Kollman PA (2015) AmberTools15.

[36]. Harris D, Loew G, and Waskell L (2001) Calculation of the electronic structure and spectra of model cytochrome P450 compound I. J. Inorg. Biochem 83, 309–318. [PubMed: 11293551]

[37]. Lindorff-Larsen K, Piana S, Palmo K, Maragakis P, Klepeis JL, Dror RO, and Shaw DE (2010) Improved side-chain torsion potentials for the Amber ff99SB protein force field. Proteins 78, 1950–1958. [PubMed: 20408171]

[38]. Eastman P, Swails J, Chodera JD, McGibbon RT, Zhao Y, Beauchamp KA, Wang LP, Simmonett AC, Harrigan MP, Stern CD, Wiewiora RP, Brooks BR, and Pande VS (2017) OpenMM 7: Rapid development of high performance algorithms for molecular dynamics. PLoS Comput. Biol 13, e1005659. [PubMed: 28746339]

[39]. McGibbon RT, Beauchamp KA, Harrigan MP, Klein C, Swails JM, Hernandez CX, Schwantes CR, Wang LP, Lane TJ, and Pande VS (2015) MDTraj: A Modern Open Library for the Analysis of Molecular Dynamics Trajectories, Biophys. J 109, 1528–1532. [PubMed: 26488642]

[40]. Tian W, Chen C, Lei X, Zhao J, and Liang J (2018) CASTp 3.0: computed atlas of surface topography of proteins. Nucleic Acids Res. 46, W363–W367. [PubMed: 29860391]

[41]. Takao H, Hirabayashi K, Nishigaya Y, Kouriki H, Nakaniwa T, Hagiwara Y, Harada J, Sato H, Yamazaki T, Sakakibara Y, Suiko M, Asada Y, Takahashi Y, Yamamoto K, Fukuyama K, Sugishima M, and Wada K (2017) A substrate-bound structure of cyanobacterial biliverdin reductase identifies stacked substrates as critical for activity. Nat. Commun 8, 14397. [PubMed: 28169272]

[42]. Brige A, Leys D, Meyer TE, Cusanovich MA, and Van Beeumen JJ (2002) The 1.25 A resolution structure of the diheme NapB subunit of soluble nitrate reductase reveals a novel cytochrome c fold with a stacked heme arrangement. Biochemistry 41, 4827–4836. [PubMed: 11939777]

[43]. Chan AC, Lelj-Garolla B, I. R. F, Pedersen KA, Mauk AG, and Murphy ME (2006) Cofacial heme binding is linked to dimerization by a bacterial heme transport protein. J. Mol. Biol 362, 1108–1119. [PubMed: 16950397]

[44]. Reniere ML, Haley KP, and Skaar EP (2011) The flexible loop of Staphylococcus aureus IsdG is required for its degradation in the absence of heme. Biochemistry 50, 6730–6737. [PubMed: 21728357]

[45]. Maines MD, and Trakshel GM (1993) Purification and characterization of human biliverdin reductase. Arch. Biochem. Biophys 300, 320–326. [PubMed: 8424666]

[46]. Ahmed FH, Mohamed AE, Carr PD, Lee BM, Condic-Jurkic K, O'Mara ML, and Jackson CJ (2016) Rv2074 is a novel F420 H2 -dependent biliverdin reductase in Mycobacterium tuberculosis. Protein Sci. 25, 1692–1709. [PubMed: 27364382]

[47]. Bashiri G, Antoney J, Jirgis ENM, Shah MV, Ney B, Copp J, Stuteley SM, Sreebhavan S, Palmer B, Middleditch M, Tokuriki N, Greening C, Scott C, Baker EN, and Jackson CJ (2019) A revised biosynthetic pathway for the cofactor F420 in prokaryotes. Nat. Commun 10, 1558. [PubMed: 30952857]

[48]. Sugishima M, Wada K, and Fukuyama K (2019) Recent Advances in the Understanding of the Reaction Chemistries of the Heme Catabolizing Enzymes HO and BVR Based on High Resolution Protein Structures. Curr. Med. Chem 26, 1–12.

[49]. Ahmed FH, Carr PD, Lee BM, Afriat-Jurnou L, Mohamed AE, Hong NS, Flanagan J, Taylor MC, Greening C, and Jackson CJ (2015) Sequence-Structure-Function Classification of a Catalytically Diverse Oxidoreductase Superfamily in Mycobacteria. J. Mol. Biol 427, 3554–3571. [PubMed: 26434506]

[50]. Chao A, Sieminski PJ, Owens CP, and Goulding CW (2019) Iron Acquisition in Mycobacterium tuberculosis. Chem. Rev 119, 1193–1220. [PubMed: 30474981]

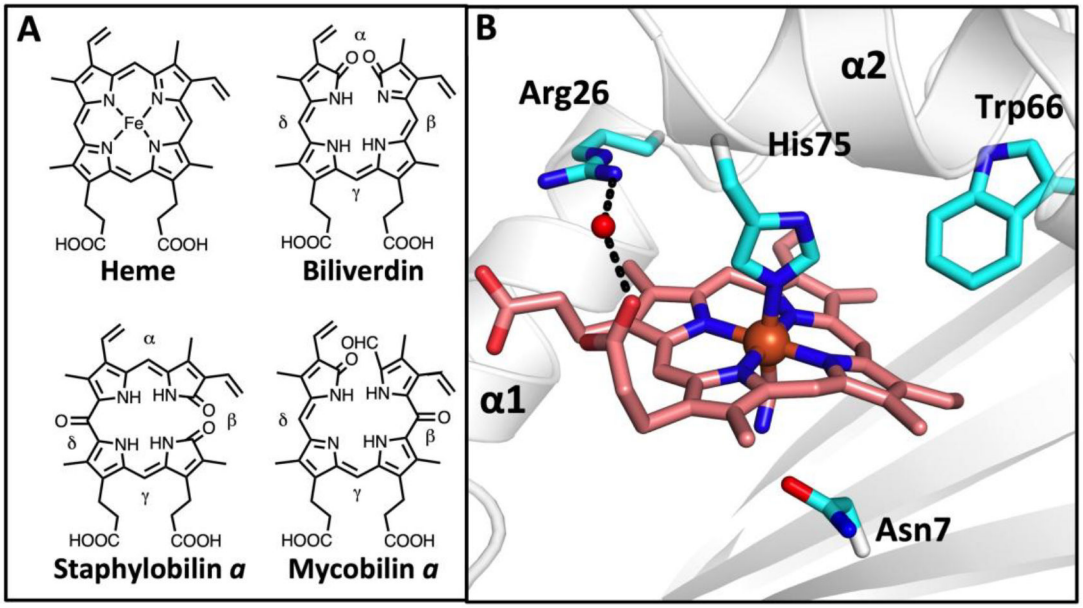

Figure 1. Structures of tetrapyrroles and WT-MhuD-monoheme.

A. The structure of heme and heme tetrapyrrole degradation products. **B**. The structure of the active site of the Mtb heme-degrading protein, MhuD (cartoon, white), in its cyano-derivatized monoheme form (stick, pink). Depicted in stick representation (cyan) are essential Asn7, Trp66 and His75 (which coordinates heme-iron) residues, and Arg26 that forms a water-mediated H-bond with one of the heme propionates.

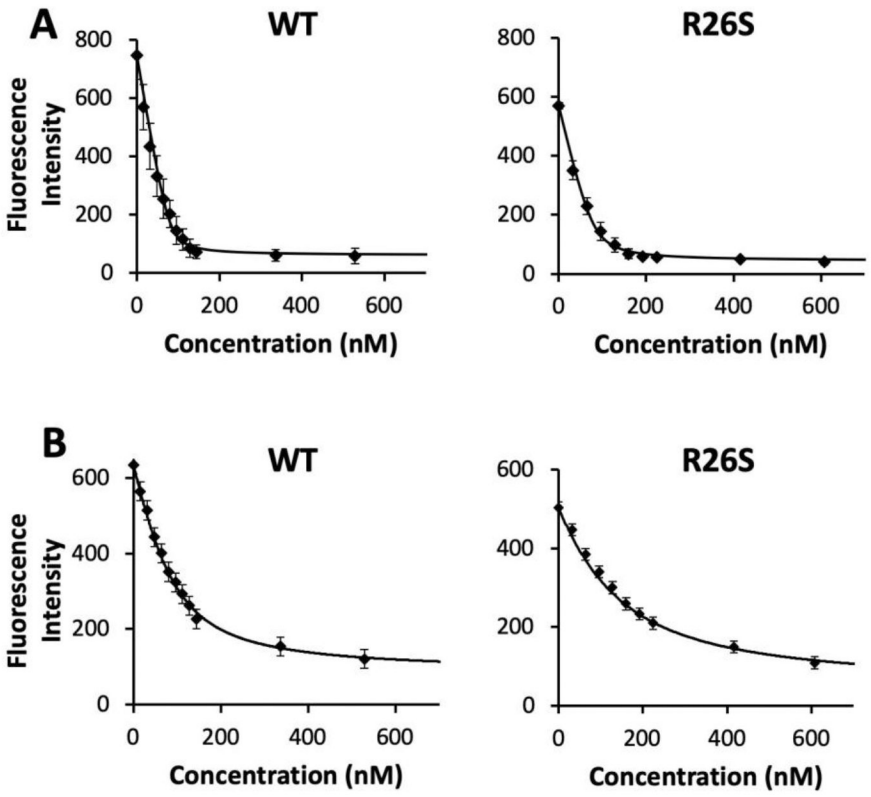

Figure 2. Heme and αBV affinity of MhuD and the R26S variant.

Representative fluorescent emission intensities at 340 nm after excitation at 280 nm of WT-MhuD (left panels) and the MhuD-R26S variant (right panels) with increasing concentrations of **A.** heme and **B.** αBV.

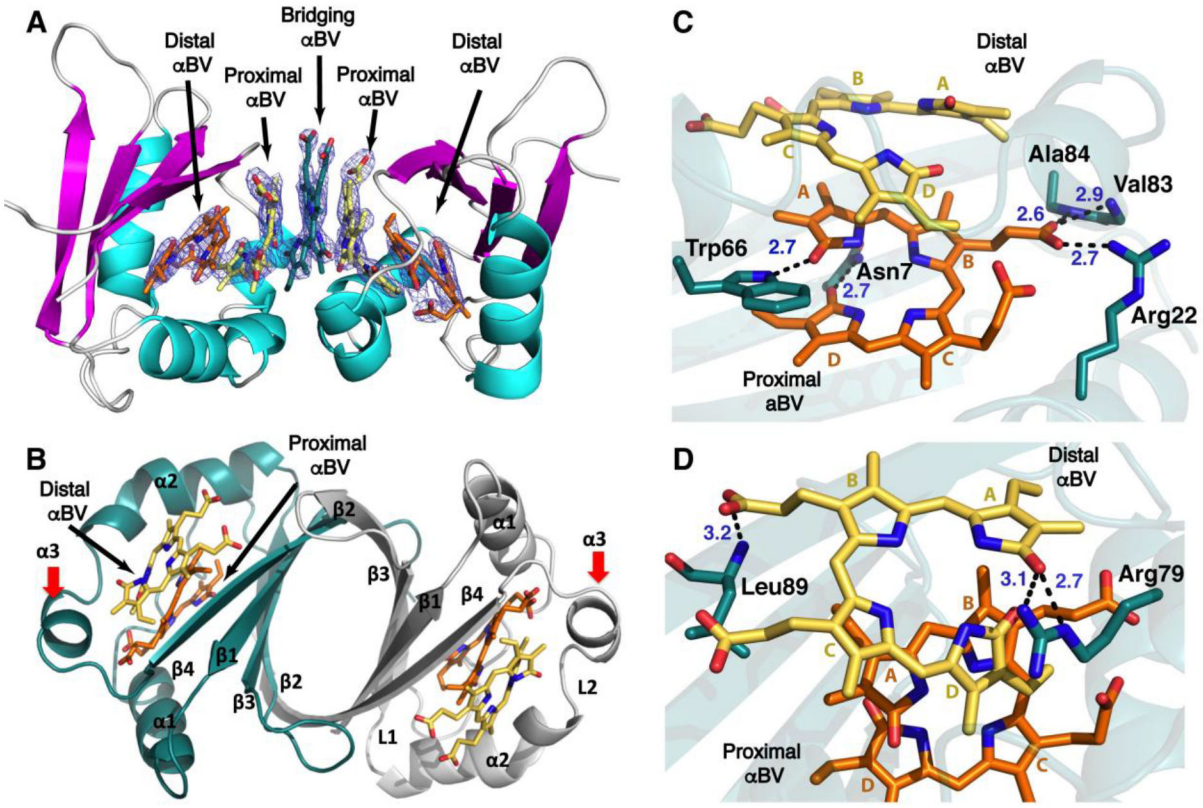

Figure 3. Structure of the MhuD-R26S-αBV complex.

A. The asymmetric unit that contains five molecules of αBV stacked connecting the active sites of two MhuD monomers. **B.** The dimeric biological assembly with two molecules of αBV per active site. The new structural helix, α3, is denoted with a red arrow. **C.** Interactions of the proximal αBV (orange) with MhuD (green). Blue dashed lines represent H-bonds with their length in Å. **D.** Interactions of the distal αBV (yellow) with MhuD (green).

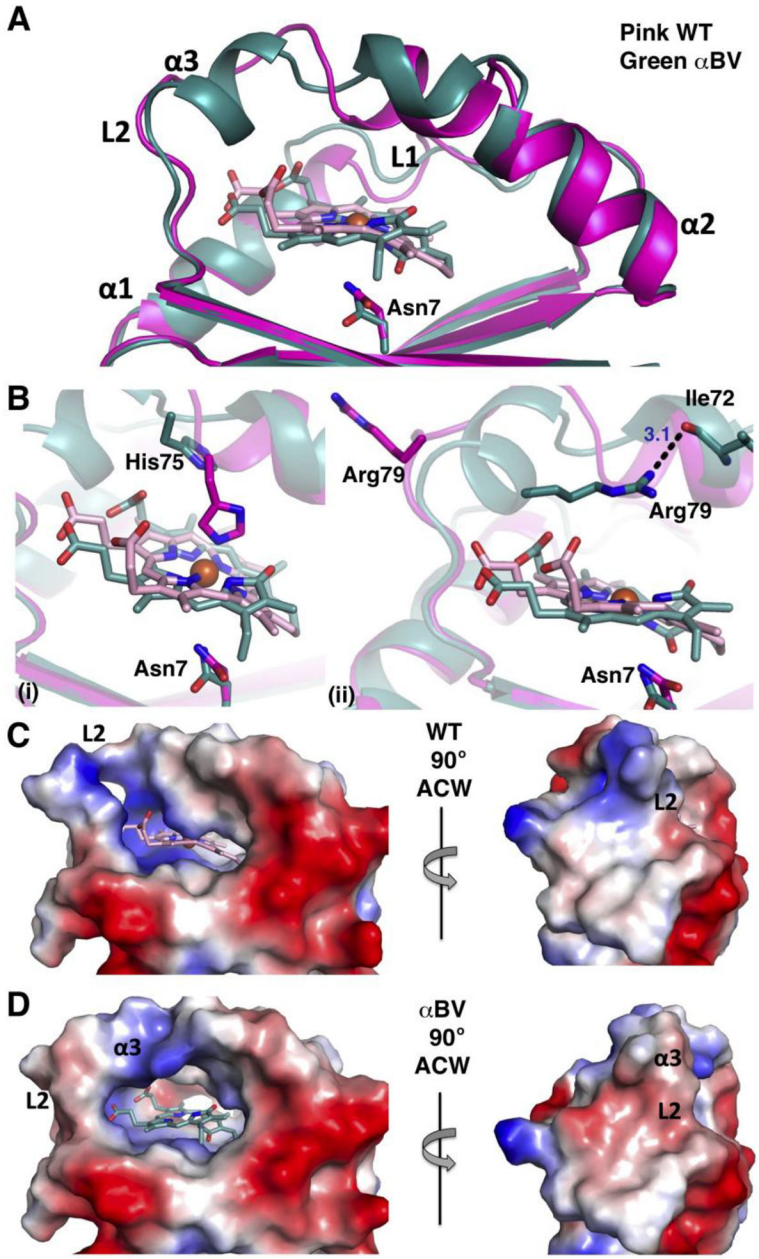

Figure 4. Structural comparison of MhuD-heme-CN and MhuD-R26S-αBV.

A. Superposition of the MhuD-heme-CN (pink, PDB ID 4NL5, the cyano group is omitted for clarity) and MhuD-R26S-αBV (green). **B**. Active site comparison with **(i)** catalytic residues Asn7 and His75, and **(ii)** residues Asn7 and Arg79, are shown in stick representation. Black dashed lines represent H-bonds with their length in Å. **C-D** Electrostatic molecular surface representations, where blue and red are positively and negatively charged surfaces, respectively. Right panel is the left panel rotated 90° anticlockwise (ACW). **C.** MhuD-heme-CN (WT) and **D.** MhuD-R26S-αBV (αBV).

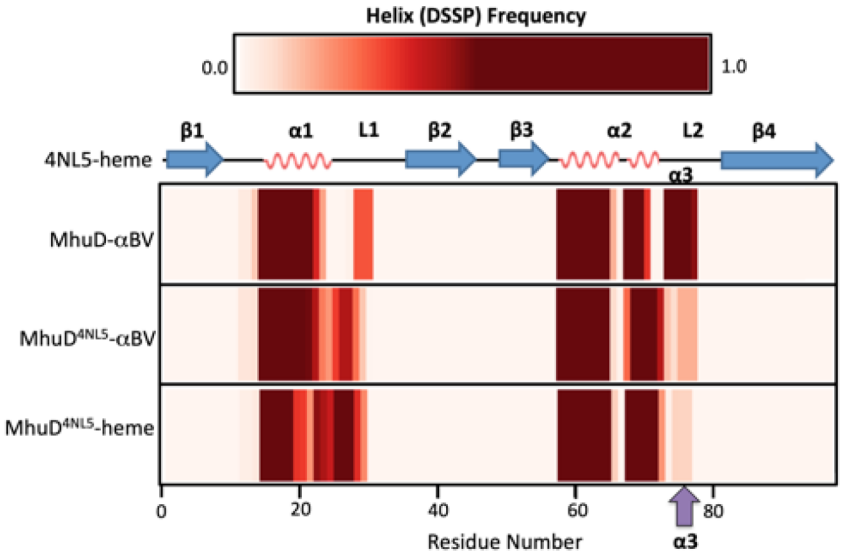

Figure 5. Helical stability in MD simulations of MhuD.

The frequency of helix formation (DSSP) is plotted for each residue of MhuD in simulations with αBV and heme. For simulations of MhuD-αBV initiated from the coordinates of the MhuD-αBV structure, the novel α-helix (α3) that forms in L2 persists. In simulations of $MhuD^{4NL5}$-αBV initiated from the coordinates of the MhuD-monoheme structure (PDB: 4NL5), α3 transiently forms in the L2 region. In the presence of heme ($MhuD^{4NL5}$-heme), formation of α3 also is observed but less frequently than in $MhuD^{4NL5}$-αBV.

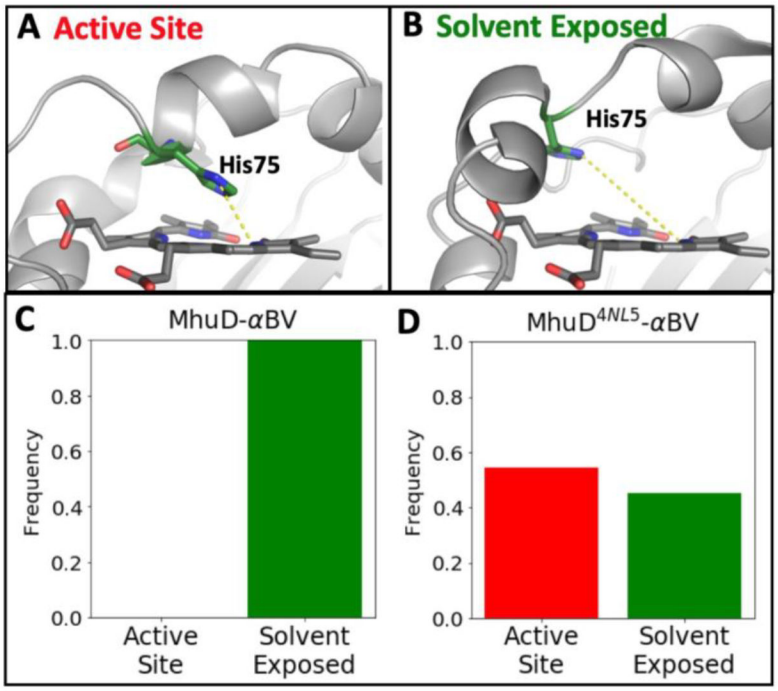

Figure 6. Orientation of His75 in MD simulations of MhuD.

During MD simulations of MhuD with αBV, the position of His75 can be classified as either a) directed into the active site or b) rotated out of the active site. This designation was assigned based on the distance between the His75 ε nitrogen atom and one of the αBV nitrogens, as described in the methods section. The structure in **A.** is a snapshot from the MhuD^{4NL5}-αBV simulation while **B.** shows a snapshot of the MhuD-αBV simulation. The frequency of each position is plotted for the MhuD-αBV simulations initiated from **C.** the MhuD-R26S-αBV crystal structure and **D.** the MhuD^{4NL5}-αBV simulations, where αBV has docked in place of heme in the MhuD-monoheme structure. For the MhuD-αBV simulations, His75 remains oriented out of the active site while in the MD of MhuD^{4NL5}-αBV, His75 flips in and out of the active site. Notably, data for MhuD^{4NL5}-heme simulations of the MhuD-monoheme structure is not shown as the His75 residue is ligated to the heme-iron and thus cannot explore alternate positions.

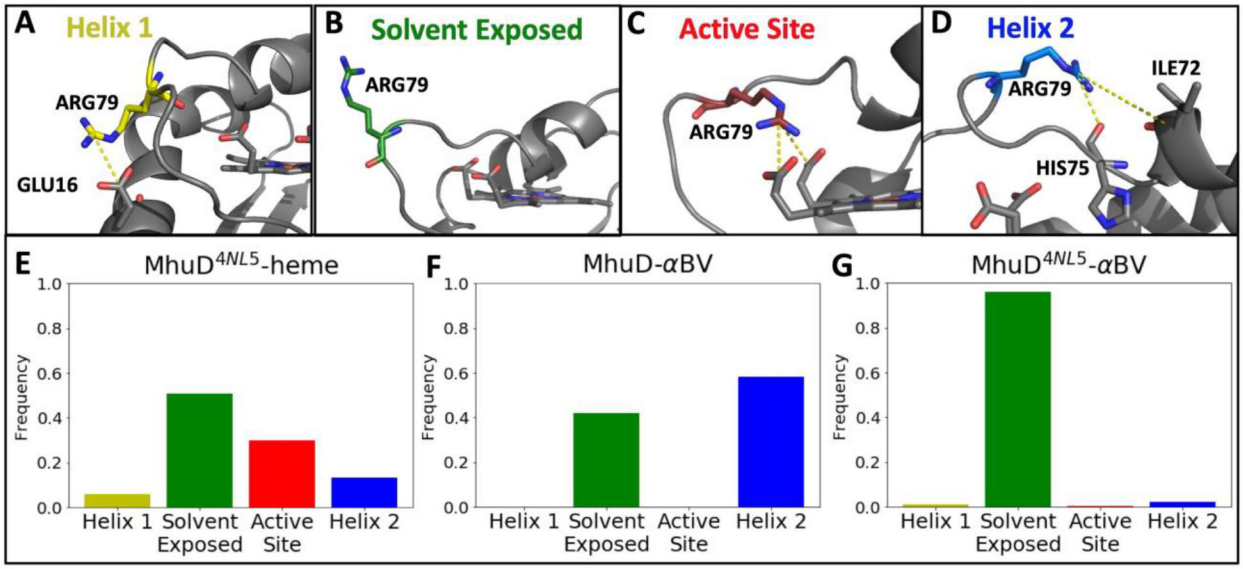

Figure 7. Position of Arg79 side-chain during MD simulations of MhuD.

In the MhuD-monoheme structure (PDB ID 4NL5), the Arg79 side-chain is unresolved. MD simulations of the MhuD- monoheme structure (MhuD^{4NL5}-heme) highlight the flexibility of this residue. We have classified its positions during simulations into four categories: **A.** *Helix 1* shows Arg79 interacting with α-helix-1 (residues 16–25), **B.** *Solvent Exposed* refers to Arg79 freely oriented in the surrounding water, **C.** *Active Site* is where Arg79 interacts with the ligand (heme or αBV), and **D.** *Helix 2* refers to the Arg79 side-chain interacting with residues in α-helix-2 (residues 60–75). All representations in **A-D** are snapshots from the simulation of MhuD^{4NL5}-heme. The frequency of each Arg79 position is plotted in panels **E-G** for all three simulation types. For **E.** MhuD^{4NL5}-heme, Arg79 is highly motile and at times, coordinates with the propionate groups of the heme ligand. For **F.** MhuD-αBV, where simulations are initiated from the coordinates of the MhuD-αBV structure, Arg79 predominantly interacts with helix 2 residues and may be stabilized by its participation in α-helix-3. For **G.** MhuD^{4NL5}-αBV, where heme has been removed from the MhuD-monoheme structure and αBV is docked in its place, the Arg79 remains mostly solvent exposed.

Table 1

Heme and αBV binding affinities (K_d) were determined for WT MhuD and the MhuD-R26S variant with 1:1 heme or αBV to protein ratio. Each experiment was performed in triplicate.

	heme K_d (nM)	**αBV K_d (nM)**
MhuD-WT	6.0 ± 2.9	36.4 ± 2.1
MhuD-R26S	9.5 ± 3.0	92.4 ± 6.8

Table 2

Statistics for X-ray diffraction data collection and atomic refinement for the MhuD-R26S-αBV complex.

Space Group	I222
Unit cell dimensions (Å)	37.22 × 113.61 × 113.65
pH of crystallization condition	6.5
Protein concentration (mg/mL)	20
Data Collection	
Wavelength, Å	1.0
Resolution range, Å	35.94 – 2.5[#]
Unique reflections (total)	8717 (120788)
Completeness, %[*]	100.00 (100.00)
Redundancy[*]	13.9 (14.4)
R_{merge}[*,†]	0.092 (0.592)
I/σ[*]	22.5 (8.9)
NCS copies	2
Model refinement	
Resolution range, Å	35.93 – 2.5
No. of reflections (working/free)	8707 (867)
No. of protein + ligand atoms	1430
No. of water molecules	16
No. of αBVs in NCS	5
R_{work}/R_{free}, %[¶]	23.16/28.53
Rms deviations	
Bond lengths, Å	0.009
Bond angles, °	1.52
Ramachandran plot	
Most favorable region, %	90.96
Additional allowed region, %	7.98
Outliers (Val30), %	1.06
PDB ID code	5J43 6PLE

[#]The data was cut off at 2.5 Å due to extreme anisotropy at high resolution.

[*]Statistics for the highest-resolution shell are given in parentheses.

[†]$R_{merge} = \Sigma_{hkl}\Sigma_i |I_i(hkl) - (I(hkl))| / \Sigma_{hkl}\Sigma_i I_i(hkl)$

[¶]$R_{work} = \Sigma|F_{obs} - F_{calc}|/\Sigma F_{obs}$. R_{free} was computed identically except where all reflections belong to a test set of 10% randomly selected data.